HAL open science

A Lagrangian Method to Isolate the Impacts of Mixed Layer Subduction on the Meridional Overturning Circulation in a Numerical Model

Matthew D. Thomas, Anne-Marie Tréguier, Bruno Blanke, Julie Deshayes, Aurore Voldoire

To cite this version:

Matthew D. Thomas, Anne-Marie Tréguier, Bruno Blanke, Julie Deshayes, Aurore Voldoire. A Lagrangian Method to Isolate the Impacts of Mixed Layer Subduction on the Meridional Overturning Circulation in a Numerical Model. Journal of Climate, 2015, 28 (19), pp.7503-7517. 10.1175/JCLI-D-14-00631.1 . hal-01233751

HAL Id: hal-01233751

https://hal.science/hal-01233751v1

Submitted on 12 Nov 2021

HAL is a multi-disciplinary open access archive for the deposit and dissemination of scientific research documents, whether they are published or not. The documents may come from teaching and research institutions in France or abroad, or from public or private research centers.

L'archive ouverte pluridisciplinaire **HAL**, est destinée au dépôt et à la diffusion de documents scientifiques de niveau recherche, publiés ou non, émanant des établissements d'enseignement et de recherche français ou étrangers, des laboratoires publics ou privés.

Distributed under a Creative Commons Attribution 4.0 International License

A Lagrangian Method to Isolate the Impacts of Mixed Layer Subduction on the Meridional Overturning Circulation in a Numerical Model

MATTHEW D. THOMAS AND ANNE-MARIE TRÉGUIER

Laboratoire de Physique des Océans, UMR 6523, CNRS-Ifremer-IRD-UBO, Plouzané, France

BRUNO BLANKE

Laboratoire de Physique des Océans, UMR 6523, CNRS-Ifremer-IRD-UBO, Brest, France

JULIE DESHAYES

Laboratoire de Physique des Océans, UMR 6523, CNRS-Ifremer-IRD-UBO, Brest, France, and International Centre for Education, Marine and Atmospheric Sciences over Africa, Department of Oceanography, University of Cape Town, Cape Town, South Africa

AURORE VOLDOIRE

CNRM-GAME (Meteo-France, CNRS), Toulouse, France

(Manuscript received 8 September 2014, in final form 13 June 2015)

ABSTRACT

Large differences in the Atlantic meridional overturning circulation (AMOC) exhibited between the available ocean models pose problems as to how they can be interpreted for climate policy. A novel Lagrangian methodology has been developed for use with ocean models that enables a decomposition of the AMOC according to its source waters of subduction from the mixed layer of different geographical regions. The method is described here and used to decompose the AMOC of the Centre National de Recherches Météorologiques (CNRM) ocean model, which is approximately 4.5 Sv (1 Sv = $10^6\,m^3\,s^{-1}$) too weak at 26°N, compared to observations. Contributions from mixed layer subduction to the peak AMOC at 26°N in the model are dominated by the Labrador Sea, which contributes 7.51 Sv; but contributions from the Nordic seas, the Irminger Sea, and the Rockall basin are also important. These waters mostly originate where deep mixed layers border the topographic slopes of the Subpolar Gyre and Nordic seas. The too-weak model AMOC can be explained by weak model representations of the overflow and of Irminger Sea subduction. These are offset by the large Labrador Sea component, which is likely to be too strong as a result of unrealistically distributed and too-deep mixed layers near the shelf.

1. Introduction

The Atlantic meridional overturning circulation (AMOC) is formed by a net northward transport of warm upper-ocean water that cools at high latitudes, descends into the deep ocean, and subsequently flows southward. The heat transported northward by the AMOC is thought to be important for European climate (Wood et al. 2003). Deep-water formation takes place mostly in the Subpolar Gyre and Nordic seas, where water becomes dense following heat loss to the atmosphere. Much of the deep branch of the AMOC (throughout the Atlantic) can therefore be traced back to high-latitude source regions where water has been subducted from the bottom of the mixed layer, the last point of contact with the atmosphere where its properties can be strongly modified. However, because of large horizontal distances and long deep-ocean travel times, it is difficult to directly study the relationship between mixed layer subduction and the AMOC in an Eulerian framework. In this study, we use Lagrangian analysis to explicitly determine the impact of

Corresponding author address: Matthew D. Thomas, Department of Geology and Geophysics, Yale University, 210 Whitney Ave., New Haven, CT 06520.
E-mail: matthew.thomas@yale.edu

DOI: 10.1175/JCLI-D-14-00631.1

© 2015 American Meteorological Society

Unauthenticated | Downloaded 11/12/21 11:59 AM UTC

mixed layer subduction on the AMOC of an ocean model so as to better understand the model circulation for comparison to observations.

Mixed layers reach their peak depth in late winter, when strong winds and convective mixing homogenize the upper layer of the water column (Williams 2001). The deepest mixed layers are mostly found away from coastal shelves in the interior ocean, particularly in the Labrador and Irminger Seas (de Boyer Montégut et al. 2004; Våge et al. 2009; Holte et al. 2010). However, convective chimneys have been shown to produce no net vertical mass transport but to only vertically mix the water column and thereby deepen the base of the unstratified mixed layer (Marshall et al. 1993; Send and Marshall 1995). Net vertical mass transfer through the base of the subpolar mixed layer and water mass transformation have instead been proposed to occur only near the basin boundary, where deep mixed layer depths (MLD) border topographic slopes (Spall and Pickart 2001; Pickart and Spall 2007). This happens during a short period of 1–2 months in March/April as the MLD shallows (Marshall et al. 1993; Qiu and Huang 1995).

Regions of mixed layer subduction thought to have the most important impact on the AMOC are situated to the north of the Denmark Strait. Observational estimates suggest approximately 6 Sverdrups (Sv; 1 Sv = $10^6\,\mathrm{m^3\,s^{-1}}$) of overflow water flows southward over the straits of the Greenland–Scotland Ridge. This subsequently entrains a further 7 Sv of ambient water to the south of the ridge, of which about 6.4 Sv occurs in the Irminger Sea (Dickson and Brown 1994; Hansen et al. 2004; Sarafanov et al. 2012). Based on a combined observational product of the high-latitude circulation in the 2000s, as well as a synthesis of earlier studies, the net contribution to the AMOC from the surface of the Irminger Sea has been estimated at approximately 3.2 Sv. This is the residual of a 10.2-Sv flux out of the mixed layer and the 6.4 Sv of entrainment that occurs below the mixed layer (Sarafanov et al. 2012). The Labrador Sea contribution to overturning has been found to be relatively small at approximately 2 Sv (Pickart and Spall 2007), although earlier estimates are as high as 8.5 Sv (see a review of these estimates by Pickart and Spall 2007). These rates are mostly based on water mass transformation and have been found to directly impact the high-latitude AMOC calculated in density space, which, while not directly comparable to a depth space calculation of AMOC, are assumed to be relevant for the AMOC in depth coordinates once the water reaches subtropical latitudes (Sarafanov et al. 2012).

Limitations in observationally derived estimates of the AMOC mean that we largely rely on ocean models to understand its latitude-dependent strength and temporal variability. Climate models are furthermore used to predict future changes in circulation and to guide policy. As such, a current problem in climate studies is the need to understand what leads to differences between the various model representations of the AMOC, which can be large (Gregory et al. 2005; Zhang and Wang 2013; Danabasoglu et al. 2014). Blanke et al. (2002) demonstrated that Lagrangian particles seeded into an ocean model can be used to calculate the overturning streamfunction. As such, endpoint information of the Lagrangian particles could be used to subsequently decompose the AMOC according to a set of proposed criteria (Döös et al. 2008). We present here a Lagrangian method for use with numerical models to diagnose which geographical regions of mixed layer subduction in the North Atlantic source the deep southward flowing water of the Subtropical Gyre and to isolate the contribution to the AMOC from the different regions. We have used the method to elucidate the circulation of the Centre National de Recherches Météorologiques (CNRM) ocean model of 1° nominal resolution (Voldoire et al. 2013; Danabasoglu et al. 2014).

In the next section, we describe the model and the Lagrangian analysis tool used here. This is followed by a description of mixed layer subduction in the model in section 3, in which the spatial and temporal characteristics of subduction are described and compared to existing studies. In section 4, we then describe the Lagrangian analysis and present the results from its application to the CNRM model. A discussion of why the model AMOC is weak is provided in section 5, along with a discussion of some limitations of the method. Finally, conclusions from the main results are given in section 6.

2. Numerical tools

a. Numerical model

In this study, we have used the CNRM global model (Voldoire et al. 2013; Danabasoglu et al. 2014), forced by the CORE-II forcing fields (Large and Yeager 2009). The model is the ocean component of the CNRM-CM5.2 coupled climate model described by Voldoire et al. (2013), which is based on the ORCA1 configuration (Hewitt et al. 2011) of the NEMO ocean model (Madec 2008) with the Global Experimental Leads and Ice for Atmosphere and Ocean (GELATO) sea ice model (Salas-Mélia 2002). The grid is tripolar with a nominal horizontal resolution of 1°. Curvature in the model grid at high latitudes means that integrated or averaged quantities along the grid, such as the AMOC, are not truly zonal but quasi zonal. At the latitude of the Denmark Strait, this distortion is approximately 2.5° (Danabasoglu et al.

Unauthenticated | Downloaded 11/12/21 11:59 AM UTC

2014). There are 42 vertical levels, staggered to give a finer surface resolution, that employ a partial step configuration to better resolve bathymetry in the bottom cell (Barnier et al. 2006). Lateral mixing of temperature and salinity is parameterized as an along-isopycnal Laplacian operator and eddy viscosity as a Laplacian with coefficient of $10^4\,m^2\,s^{-1}$. The eddy-induced velocity is parameterized according to the Gent and Mcwilliams (1990) scheme. Lateral boundaries are free-slip, bottom boundaries that employ a nonlinear friction with coefficient of $10^{-3}\,m^2\,s^{-1}$, and the Beckmann and Döscher (1997) diffusive bottom boundary layer scheme is used with coefficient of $10^4\,m^2\,s^{-1}$. The straits of the Greenland–Scotland Ridge have been deepened and widened artificially to facilitate overflow. The CORE-II forcing is version 2 of the CORE dataset (Large and Yeager 2009; http://rda.ucar.edu/datasets/ds260.2/#!description), which is 60 years long, between 1948 and 2007, and which incorporates NCEP reanalyses of near-surface atmospheric temperature, wind, specific humidity, and density, as well as satellite-derived sea surface temperature, precipitation, and sea ice concentration.

We use monthly output from a 300-yr simulation that is composed of five cycles of CORE-II forcing initialized from Levitus rest state. To avoid any residual spinup, we use only the final 180 yr of the simulation. The long run time and realistic climatic (including extreme) events make the model particularly useful for the purposes of studying the production and transport of deep water. Model March-mean MLDs in the North Atlantic, as calculated according to a turbulent kinetic energy scheme (Blanke and Delecluse 1993; Fig. 1a), are too deep in the Subpolar Gyre in comparison to the Argo float-based calculations of Holte et al. (2010; Fig. 1c). In the Labrador Sea, in particular, the MLDs are also unrealistically distributed, being deepest close to the continental slope, as opposed to the central Labrador Sea (de Boyer Montégut et al. 2004; Våge et al. 2009; Holte et al. 2010). The coupled version of this model, CNRM-CM5.2, displays a more realistic Labrador Sea March-mean MLD, indicating that the problem lies either with the forcing or with unrealistic atmosphere–ocean–ice feedbacks. The model time-mean Eulerian AMOC, calculated as the depth-integrated and basinwide zonally integrated meridional velocities (Fig. 2a), is about 4.5 Sv weaker than the 18.5 Sv estimated at 26°N from observations made at the RAPID array (Kanzow et al. 2007; McCarthy et al. 2012). As is typical for models, the CNRM AMOC is also shallower than observed by the RAPID array (Danabasoglu et al. 2014). Note that, for consistency with the Lagrangian particle tracks described later, the Eulerian AMOC calculation here includes the circulation of the Mediterranean Sea and the Black Sea. For more information regarding the model,

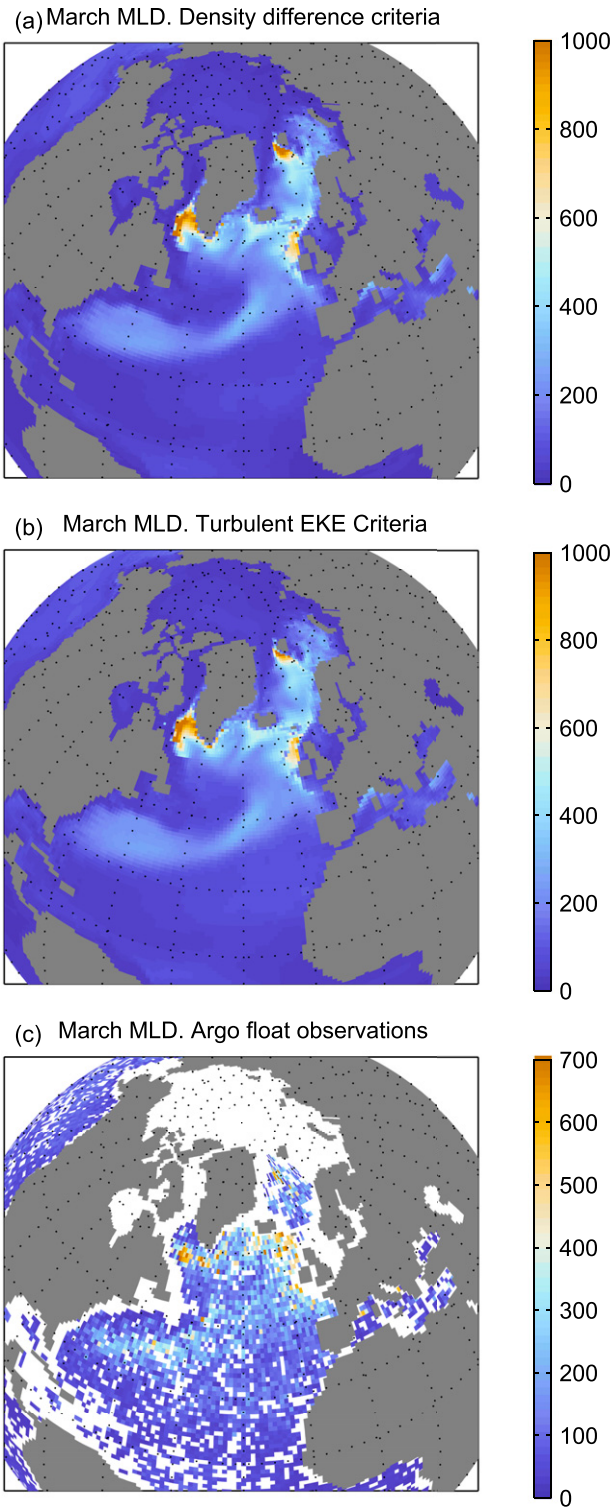

FIG. 1. March-mean mixed layer depth (m) as determined according to (a) a surface-referenced potential density-threshold difference of $0.01\,kg\,m^{-3}$ between the mixed layer depth and the surface, (b) the model turbulent kinetic energy scheme, and (c) observational estimates from Argo data by Holte and Talley (2009). For practical purposes, the density difference method is used throughout this study.

Unauthenticated | Downloaded 11/12/21 11:59 AM UTC

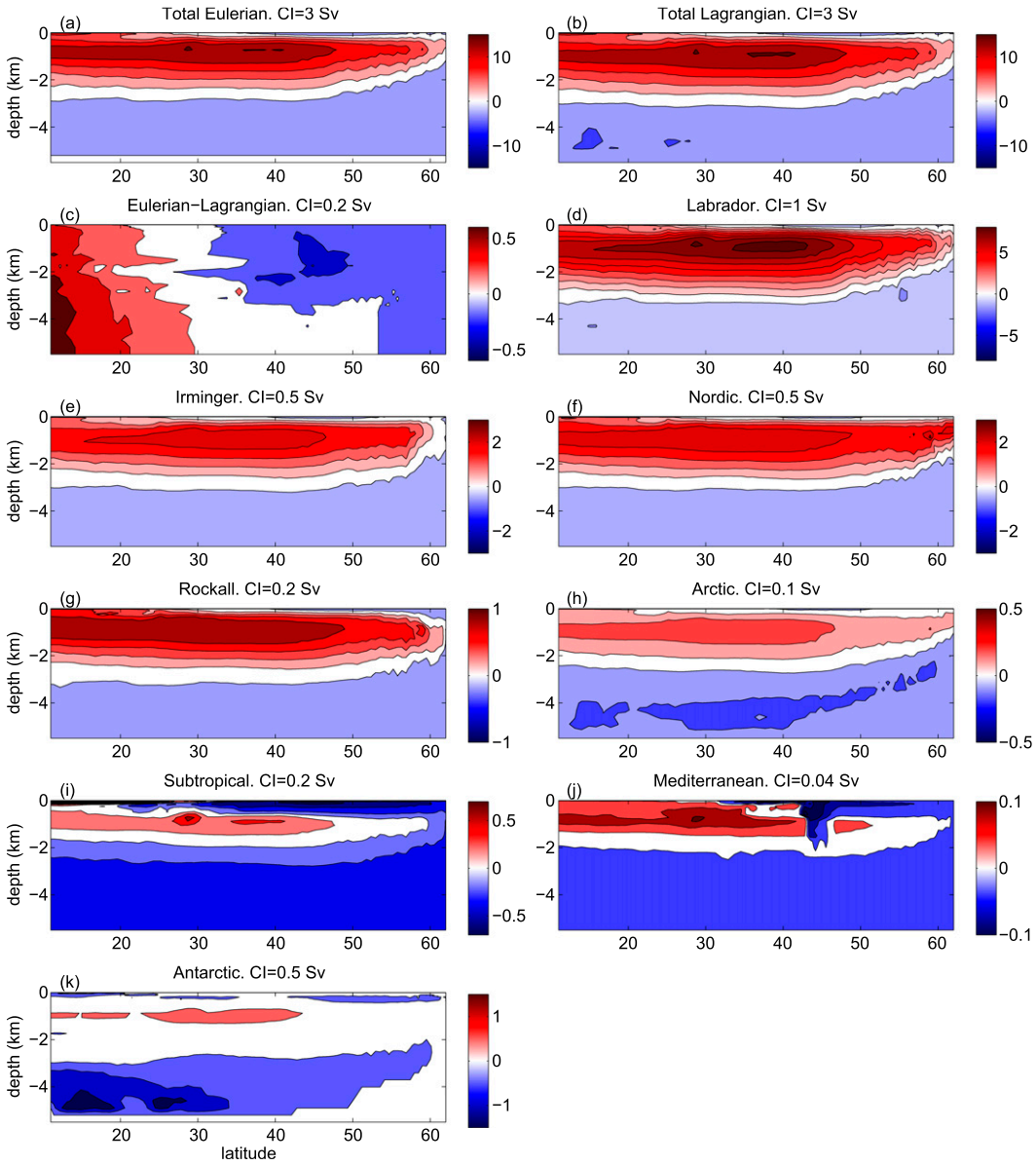

FIG. 2. The time-mean AMOC streamfunctions (Sv) according to the (a) Eulerian and (b) Lagrangian calculations and (c) their difference. (d)–(j) Component contributions (Sv) to the AMOC from subduction from the mixed layer depth of the various subdomains: (d) the Labrador Sea, (e) the Irminger Sea (f) the Nordic seas, (g) the Rockall basin, (h) the Arctic Ocean, (i) the Subtropical Gyre, and (j) the Mediterranean Sea. (k) The component contribution (Sv) from Antarctic Bottom Water (recirculated water that has not interacted with the mixed layer). The sum of the components (d)–(k) match the full Lagrangian streamfunction in (b). See Fig. 6 for the geographical boundaries of the subdomains. The latitude shown is the mean latitude along each latitude index, which is increasingly curved at higher latitudes. The contour interval (CI) for each plot is marked in the titles.

we refer the reader to Voldoire et al. (2013) and also to Danabasoglu et al. (2014), who compare the model to a suite of other CORE-II-forced models.

b. *Lagrangian analysis tool*

We have used the Lagrangian analysis tool Ariane (http://www.univ-brest.fr/lpo/ariane), which integrates particle trajectories in time according to three-dimensional model output velocity fields (Döös 1995; Blanke and Raynaud 1997). Particles can be initiated along any number of definable sections or surfaces, be they either flat vertical or horizontal cross sections or time-dependent isolines of a chosen quantity. Each particle can be seeded on the face of a grid cell and assigned a

Unauthenticated | Downloaded 11/12/21 11:59 AM UTC

volume transport that is subsequently conserved through time. They are thus nondissipative by construction, thereby allowing the total Eulerian transport across a surface to be fully allocated to a suite of particles and subsequently traced to their respective final destinations. The number of seeded particles per grid cell is set by a constraint that limits the maximum transport that a particle can be assigned. If the transport across a cell face exceeds this limit, then it is subdivided evenly along the two spatial dimensions and the time dimension until each particle (one per subdivision) satisfies the constraint [for a complete description of the subdivision, the reader is referred to section 2c of Blanke et al. (1999)]. Particle velocities, temperatures and salinities change through the time integration according to the local Eulerian model fields. Particles are integrated until they reach any one of a number of specified final sections. Here their time integration is stopped and their final properties are stored. In this manner, relationships between the initial and final sections can be quantified. As with the initial sections, the final sections can be either a simple cross section that is fixed in time, such as a set of geographical sections that together form the boundary of a domain, or/and a more complex definition that satisfies some specified criterion based on a physical or temporal constraint.

In the Lagrangian experiments performed in this study, particles have been run in a North Atlantic/Arctic domain bounded by vertical cross sections that are zonally situated along 10°N in the Atlantic and along the Bering Strait at 65°N in the Pacific. The domain includes the Mediterranean and Black Seas. Particles were initiated along the 10°N cross section at each time step of the 180-yr time series and then integrated backward in time. The methodology only propagates particles within the domain. Only particles with southward velocity are therefore seeded such that the full southward transport across the section during each of the initializing time steps is assigned among the suite of initialized particles. The backward time integration for a particle is then complete once the particle intercepts one of the two domain boundaries. Since we only follow those particles with initial southward velocity, we here only calculate the time-mean, and not time-dependent, AMOC. Future iterations of the method could, however, be made to extract the temporal variability (see discussion section). The time-mean AMOC is generated once the full spatial and temporal distribution of velocities has been sampled by the particles. Individual particle transports have been limited to be less than an upper threshold of 0.1 Sv, which in our case results in some 3.8 million particles. To avoid the excessive storage requirements of saving the particle properties at each point along their trajectory, Ariane can be run in a so-called quantitative mode that outputs only the end-point characteristics as well as the mean statistics and streamfunctions of the trajectories. Should further savings on storage or processing be required for any future uses of the method, we note that none of the major conclusions of the manuscript are modified if we instead seed the minimimum number of particles (i.e., one particle per grid cell face per time step along 10°N), nor if we reduce the seeding period to only a 50-yr period. Our results change very little with an increase in the number of seeded particles.

To achieve the long time periods of overturning, which greatly exceed the 180 yr of model output, we have allowed the particles to loop in time over consecutively looped model output. We allowed for up to 10 cycles (1800 yr), after which over 99.8% of the particles had been intercepted at one of the domain boundaries. This has potentially introduced a sharp transition at each successive loop that can cause an unphysical jump in the particle trajectories. To verify that this transition does not impact our main conclusions, we have performed an additional experiment (the same as described in section 4b later) in which we have added two artificial jumps into the time series by reorganizing the time series so that the relative years 121–180 occur before the years 61–120. None of the values reported later are sensitive to the introduction of these two additional jumps. By running the particles offline according to the monthly mean model output, we further introduce an error that is related to the nonlinear terms in the momentum equations. In a model of 2° nominal resolution, Valdivieso Da Costa and Blanke (2004) assessed the sensitivity of particle trajectories to the temporal resolution of the output. They found that the use of monthly output introduced individual trajectory errors of up to 8% of the distance traveled, relative to a control run with output frequency of 15 h. Since our model also does not resolve eddies, we assume this error to be representative of our study to first order. The lack of sensitivity of the results to the number of seeded particles, as described above, is evidence that this is not an important source of error here.

3. Mixed layer subduction

Here we describe the spatial and temporal distributions of mixed layer subduction in the North Atlantic/Arctic domain. This is used to both verify the accuracy of the model representation of subduction as compared to existing studies, and to compare to later results that identify the regions of subduction that contribute to the model AMOC. For practical reasons concerning the designation of an MLD in Ariane (which we use later to

Unauthenticated | Downloaded 11/12/21 11:59 AM UTC

decompose the model AMOC), we here and throughout the rest of the manuscript use a definition of the MLD based on a simple density-threshold criterion. Unless stated otherwise, the MLD is henceforth defined as the shallowest depth that exhibits a surface-referenced potential density exceeding the surface value by 0.01 kg m^{-3}. The March-mean MLD of this density-threshold-based criterion is shown in Fig. 1a. The 0.01 kg m^{-3} threshold is chosen, as it produces an MLD with a North Atlantic spatial distribution that similarly resembles that determined from the model turbulent kinetic energy criterion (Fig. 1b).

To determine mixed layer subduction, we calculate the net subduction velocity across the time-evolving MLD at each time step according to

$$S = -\partial h/\partial t - \mathbf{u}_b \cdot \nabla h - w_b, \qquad (1)$$

where h is the depth of the mixed layer, and $\mathbf{u}_b$ and w_b are the horizontal and vertical velocities at the base of the mixed layer, respectively (Williams 2001; Valdivieso Da Costa et al. 2005). Time-mean rates of S are shown in Fig. 3c, the sum of the time-mean rates of subduction out of the mixed layer (positive S; Fig. 3a) and the obduction into the mixed layer (negative S; Fig. 3b). Spatial distributions of subduction and obduction rates both resemble the spatial pattern of the March-mean mixed layers throughout the domain (Fig. 1). The values also qualitatively resemble those calculated using an ocean data assimilation product (Liu and Huang 2012), although their values were calculated relative to the MLD [i.e., they did not contain the first term on the RHS of Eq. (1)] and cannot be compared directly. Net subduction and obduction largely cancel out in many places to leave a residual distribution of S where strong net subduction occurs only close to topographic boundaries. The distribution and values are qualitatively similar to those calculated by Valdivieso Da Costa et al. (2005, their Fig. 2) in a 1/6° model, though in our model, subduction persists around the full edge of the Labrador Sea. A diagnosis of the time-mean terms in Eq. (1) reveals that net S at high latitudes is primarily caused by horizontal fluxes out of the mixed layer (the second term on the RHS; Fig. 4). This agrees with Marshall et al. (1993), who calculated subduction terms from observed climatology, although the values presented here are larger at subpolar latitudes, perhaps because of differences in methodology (for differences between the instantaneous kinematic approach, as is used here, with one based on climatology, the reader is referred to Valdivieso Da Costa et al. 2005). Away from the boundaries, there is net subduction in the interior Subtropical Gyre and net obduction in the Subpolar Gyre,

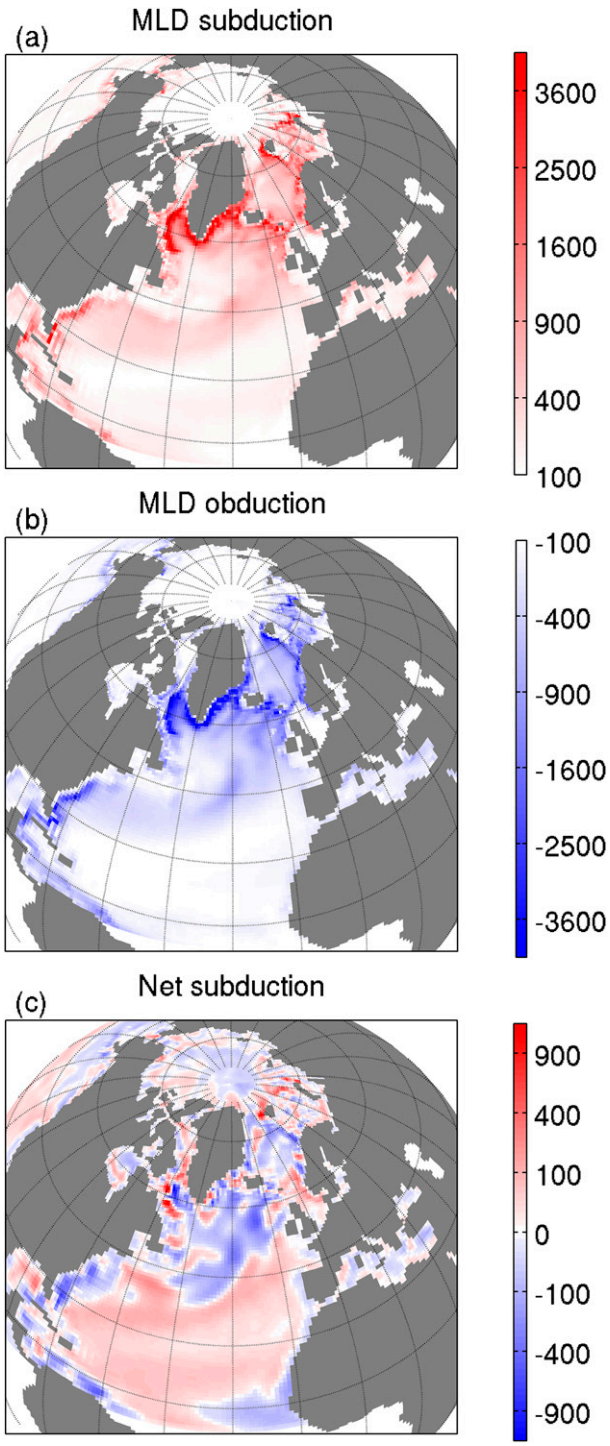

FIG. 3. Time-mean rates (m yr^{-1}) of (a) subduction (positive S), (b) obduction (negative S), and (c) their difference S [see Eq. (1)] calculated each month at the base of the time-dependent mixed layer. Positive values of S represent a net subduction. Values have been scaled as a quadratic and smoothed with a radius of 1 grid cell to reduce small-scale noise.

Unauthenticated | Downloaded 11/12/21 11:59 AM UTC

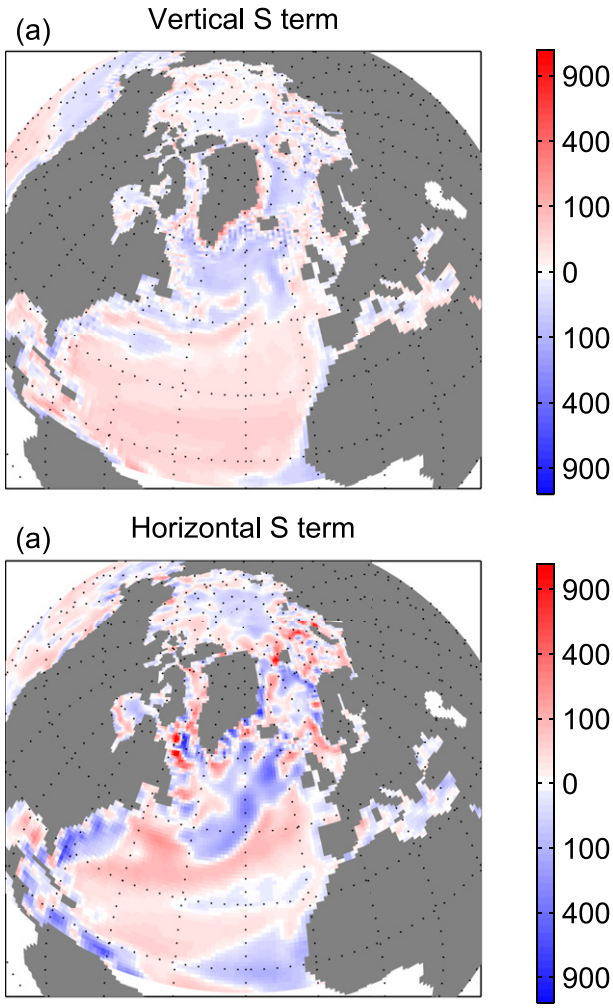

FIG. 4. Time-mean rates (m yr^{-1}) of net S due to (a) vertical fluxes out of the mixed layer [the third term on the RHS of Eq. (1)] and (b) horizontal fluxes out of the mixed layer [the second term on the RHS of Eq. (1)]. The contribution from vertical fluctuations of the MLD [the first term on the RHS of Eq. (1)] is negligible. Positive values represent a net subduction. Values have been scaled as a quadratic and smoothed with a radius of 1 grid cell to reduce small-scale noise.

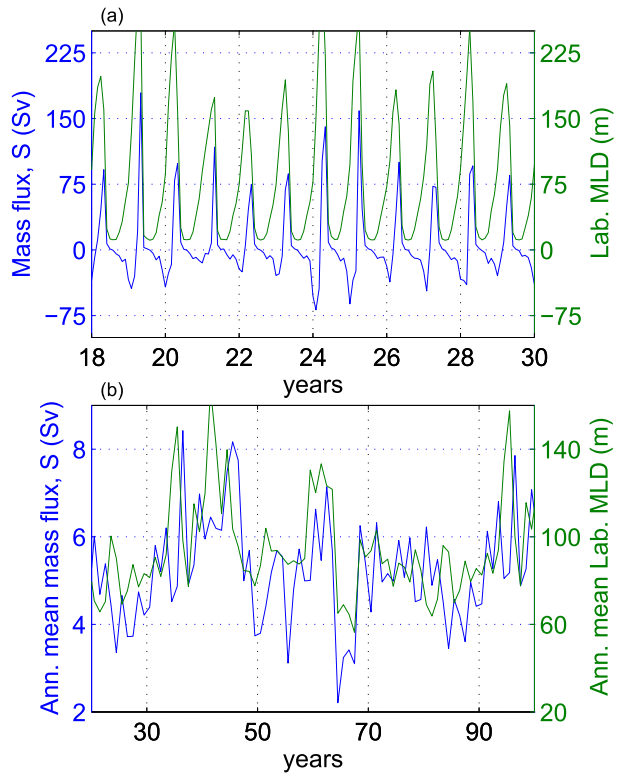

FIG. 5. (a) Monthly and (b) annually averaged time series of S (blue curves; left axes; Sv) and mixed layer depth (green curves; right axes; m) horizontally integrated and averaged, respectively, over a Labrador Sea domain between longitudes 65° and 45°W and latitudes 52° and 70°N. The time-mean S is 5.2 Sv. Positive values of S represent a net subduction. For clarity, only portions of the time series are shown. Model years are relative to the first model year.

consistent with the Ekman pumping and Ekman suction in the gyres respectively (Williams 2001). Cancelation between subduction and obduction occurs because of seasonal deepening and shoaling events of the mixed layer that entrain and subsequently release water over the duration of a winter. Note that regions of net subduction do not necessarily imply that these are the same regions that supply water to the AMOC, since subducted water may simply obduct back into the mixed layer before leaving the Subpolar Gyre. In the following section, we address which regions of subduction are important for the AMOC.

The time-mean S, when integrated over a large domain, is relatively small. Spatially integrating over a Labrador Sea domain, between longitudes 65° and 45°W and latitudes 52° and 70°N, produces a net subduction of approximately 5.2 Sv out of the mixed layer, the residual of cancelling positive and negative transports that are distributed horizontally over the region. This residual transport is also the result of a strongly cancelling seasonal cycle. A time series of S integrated over the same domain reveals large monthly rates peaking at about 200 Sv (Fig. 5a). The first term on the RHS of Eq. (1) is almost entirely responsible for these fluctuations. The timing and strengths of S are therefore dependent on the MLD, with obduction occurring in early winter as the mixed layer deepens and entrains fluid, and subduction in late winter as the mixed layer shoals (Qiu and Huang 1995). Similarly strong seasonal fluctuations of S have also been reported in the Subtropical Gyre from an eddying model (Valdivieso Da Costa et al. 2005). Annual-mean values of S (calculated from September to August) are substantially smaller (Fig. 5b). Obduction and subduction peaks over a single wintertime period

Unauthenticated | Downloaded 11/12/21 11:59 AM UTC

TABLE 1. Peak AMOC transports of the Eulerian, the Lagrangian, and the Lagrangian components of the model AMOC at 26°N (second column), the depth at which the peak AMOC transport occurs (third column), and the AMOC transport at 881-m depth (the depth at which the full AMOC peaks; fourth column), calculated using an MLD threshold of 0.01 kg m^{-3} density difference relative to the surface. The different AMOC calculations and components are listed in the first column, of which the geographical limits are shown in Fig. 6. Numbers in parentheses represent the values obtained when MLD thresholds of 0.001, 0.003, 0.005, and 0.02 kg m^{-3} are used, respectively.

26°N component	Peak AMOC streamline (Sv)	Depth of peak streamline (m)	AMOC streamline at 881m (Sv)
Eulerian	14.03	881	14.03
Lagrangian	13.92	881	13.92
Antarctic	−1.21 (−1.22, −1.22, −1.22, −1.21)	4603 (4603, 4603, 4603, 4603)	0.53 (0.80, 0.67, 0.62, 0.44)
Arctic	0.23 (0.19, 0.21, 0.22, 0.22)	881 (881, 881, 881, 881)	0.23 (0.19, 0.21, 0.22, 0.22)
Nordic	2.16 (2.81, 2.55, 2.40, 1.88)	1062 (1062, 1062, 1062, 1062)	2.16 (2.80, 2.55, 2.40, 1.88)
Labrador	7.51 (5.81, 6.45, 6.84, 8.41)	881 (881, 881, 881, 881)	7.51 (5.81, 6.45, 6.84, 8.41)
Irminger	2.11 (2.50, 2.40, 2.30, 1.82)	881 (881, 881, 881, 881)	2.11 (2.50, 2.40, 2.30, 1.82)
Rockall	0.92 (1.17, 1.07, 1.02, 0.78)	881 (881, 881, 881, 881)	0.92 (1.17, 1.07, 1.02, 0.78)
Subtropical	0.68 (0.73, 0.70, 0.69, 0.66)	40 (40, 40, 40, 40)	0.37 (0.53, 0.46, 0.42, 0.29)
Medsea	0.09 (0.12, 0.11, 0.10, 0.08)	881 (881, 881, 881, 881)	0.09 (0.12, 0.11, 0.10, 0.08)

therefore mostly cancel (Fig. 5b). As with the time-mean S, annual-mean S is dominated by the second term on the RHS of Eq. (1). A comparison between annual-mean S and annual-mean MLD in the Labrador Sea shows that the two are reasonably well correlated at 0.49 (Fig. 5b). This increased to 0.73 when a small spatial averaging domain was instead taken over a region of net subduction. Deeper mixed layers in the Labrador Sea therefore lead to more subduction, which we suggest is because of modifications to the slope of the mixed layer depth [Eq. (1)]. We would like to stress, however, that the unrealistic distributions and depths of the March-mean mixed layer in the model indicate that these values may not be representative of the real ocean.

4. Lagrangian analysis of the AMOC

a. Lagrangian AMOC

If the model transports have been well sampled by the trajectories of the particles described in section 2b, zonal and vertical summations over the particle transports can be taken to build the full latitude-depth time-mean AMOC streamfunction of the model within the Atlantic/Arctic domain (Döös 1995; Blanke et al. 2002; Döös et al. 2008). The Lagrangian AMOC streamfunction generated for CNRM (Fig. 2b) compares well with the Eulerian calculation (Fig. 2a). The streamfunction at the sea floor is not zero because of an approximately 1.7-Sv transport into the domain through the Bering Strait that ensures that there is not a closed mass balance. The discrepancy between the Lagrangian and Eulerian calculations peaks at approximately 0.6 Sv in the lower domain latitudes and is typically less than 0.4 Sv throughout the domain, which we consider to be small (Fig. 2c).

b. Lagrangian decomposition of the AMOC

We now detail the methodology of the Lagrangian AMOC decomposition and describe the results of its application to the model output. The method decomposes the AMOC into component latitude-depth streamfunctions. Each streamfunction is associated either with the impact of mixed layer subduction from one of a set of geographically distributed subdomains, or with circulation that starts and ends at the 10°N cross section. The linear sum of the component streamfunctions makes up the full Lagrangian AMOC streamfunction (Fig. 2; Table 1). Using the backward particle trajectories described in section 2b, the method works generally by first categorizing the particles according to a set of criteria, with each criterion associated with either subduction from a geographical subdomain or with recirculation back to 10°N. Particles from each criterion can then be isolated, and their component contributions to the full Lagrangian streamfunction can be calculated by zonally and vertically summing over their combined trajectories.

In more detail, the methodology can be split into three main steps:

1) Determine the mixed layer origins of the 10°N particles: After their release from 10°N, each particle is then tagged at the position where they last subducted from the time-dependent mixed layer (the last point of contact with the atmosphere). Figure 5 shows the distribution of where particles last subducted from the mixed layer, plotted as a mean rate of subduction that we dub S_{10N}. We have regridded rates of S_{10N} onto a regular 1° grid for convenience. In broad agreement with net subduction S (Fig. 3c), regions of strong S_{10N} at high

Unauthenticated | Downloaded 11/12/21 11:59 AM UTC

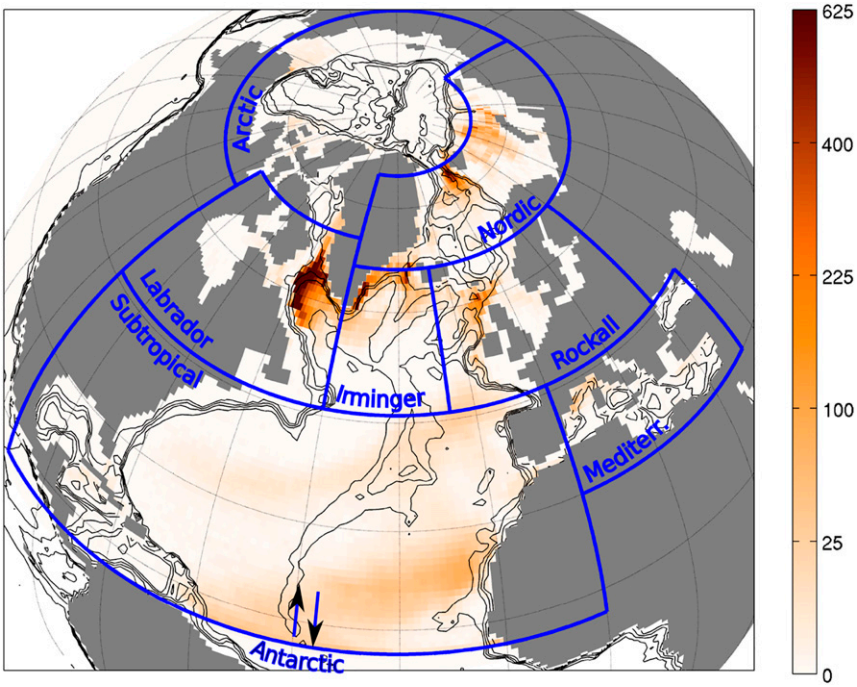

FIG. 6. Mixed layer subduction rate (m yr^{-1}) of water that ends at 10°N S_{10N}, as determined from backward particle trajectories from 10°N that are intercepted at the time-dependent MLD. Contours show the model bathymetry from 500 to 3500 m in intervals of 1000 m. Blue boxes show the boundaries of the chosen subdomains within which the net impact of mixed layer subduction on the AMOC is isolated. These are the Subtropical Gyre, Mediterranean Sea, Labrador Sea, Irminger Sea, Rockall basin, Nordic seas, and Arctic Ocean subdomains. The Antarctic label and arrows refer to Lagrangian particles that circulate from and back to 10°N without interacting with the mixed layer depth. Colors have been scaled as a quadratic.

latitude, which ultimately source the AMOC, are predominantly located around the edges of the Subpolar Gyre and Nordic seas and are generally located where deep MLDs border topography (Fig. 1b). This is similar to regions where net sinking (Böning et al. 1996; Spall and Pickart 2001) and water mass transformation (Pickart and Spall 2007) have been found to occur.

2) Split the AMOC into components according to different geographical regions of S_{10N}: The North Atlantic domain is split into subdomains, consisting of subtropical, Labrador, Irminger, Rockall, Nordic, Arctic, and Mediterranean subregions, the boundaries of which are delineated as shown in Fig. 6. The particles that subducted from the mixed layer of each of these regions (at the rates of S_{10N} shown in Fig. 5) are then grouped, and the component contributions to the AMOC from each group are separately calculated (Figs. 2d–j). [As a practical note for any future uses of the methodology, the procedure for tagging particles at the base of the MLD, grouping them, and then decomposing their AMOC contributions is as follows: backward particle integrations from 10°N are first run while applying a constraint that terminates their integrations when their density becomes within 0.01 kg m^{-3} of the surface value (i.e., at the base of the MLD). This allows the particles to be grouped into the different geographical subdomains according to where they last subducted, but component overturning streamfunctions cannot yet be calculated because the particles have been prevented from following the upper branch of the AMOC. To calculate the AMOC components, the time integrations are then repeated separately for each group of particles, but now without the mixed layer constraint. This therefore allows the particles of each group to reach the control sections and their component streamfunctions to be separately calculated by zonally and vertically summing over their combined trajectories.]

3) Determine the component streamfunction for particles that do not interact with the MLD (Fig. 2k): A large fraction of the particles start and end at 10°N without ever interacting with the MLD. These particles are composed of short-lived particles that

Unauthenticated | Downloaded 11/12/21 11:59 AM UTC

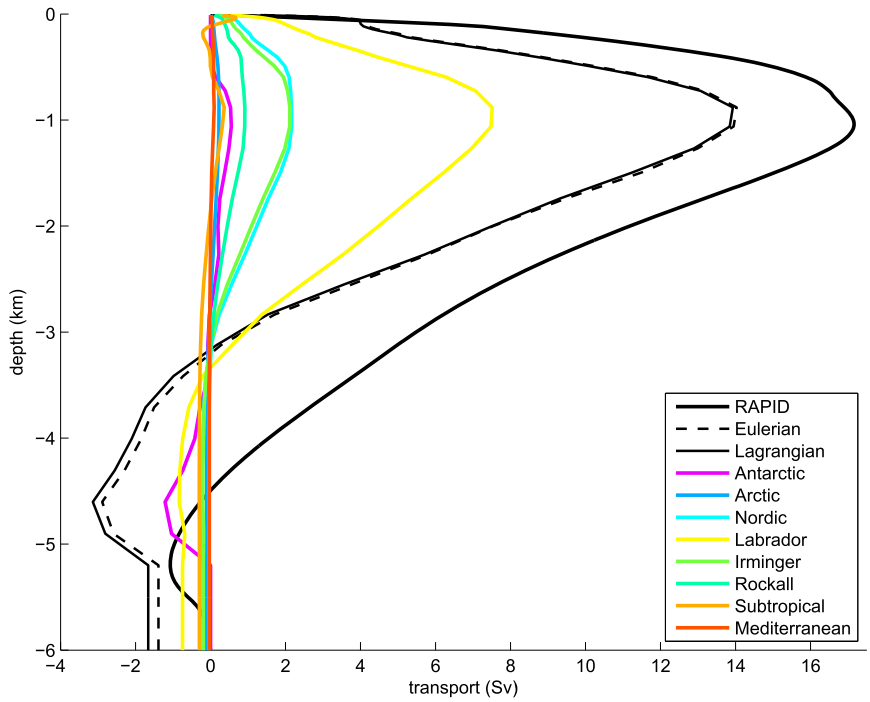

FIG. 7. The time-mean AMOC northward transports (Sv) at 26°N, cumulatively integrated from the surface downward. Transports are shown for the Eulerian AMOC calculation and for the Lagrangian AMOC calculation and its component contributions from Antarctic Bottom Water (recirculated water that has not interacted with the MLD), as well as subducted water from the MLD of the various subdomains: Arctic Ocean, Nordic seas, Rockall basin, Irminger Sea, Labrador Sea, Subtropical Gyre, and Mediterranean Sea. The AMOC transports from the RAPID array are also shown. The sum of the components matches the full Lagrangian streamfunction. Component contributions to the AMOC are summarized in Table 1. See Fig. 6 for the geographical boundaries of the subdomains.

recirculate back to 10°N with very little contribution to overturning, and of Antarctic Bottom Water that enters the domain at depth and recirculates back with a negative contribution to the streamfunction. We therefore call this the Antarctic component, which at 26°N peaks at −1.21 Sv at 4603-m depth (Fig. 7). There is a small middepth positive overturning cell in the Antarctic component that peaks in subtropical latitudes at 0.53 Sv, which is probably not related to Antarctic Bottom Water but instead to water that recirculates back to 10°N at middle depths. While there is a very small fraction of particles of Bering Strait origin that never pass through the mixed layer, their contribution is negligible and ignored here.

The component latitude-dependent streamfunctions are shown in Fig. 2, and their values at 26°N are displayed in Table 1 and in Fig. 7 along with the observed estimate from the RAPID array (Cunningham et al. 2007). Unlike in our model, the RAPID streamfunction has been adjusted to balance mass. Note that, while the peak AMOC contributions at 26°N are not constrained to exactly equal the spatially integrated values of S_{10N} from each domain, the values compare very closely for the high-latitude domains since almost all of the subducted water from here overturns. Each component has a small residual offset in the streamfunction at the sea floor because of a portion of the water of Bering Strait origin that last subducts in each subdomain. Latitudinal variations in each of the component streamfunctions are due to differing degrees of both zonal cancellation in the zonal integrals and in recirculation of the particles. By far, the largest component contribution is from the Labrador Sea, with a peak of 7.51 Sv. This is stronger than the 5.2-Sv net Eulerian subduction S calculated in the Labrador Sea (see section 3), however the calculation of S is more sensitive to the size of the domain because it includes obduction. Other significant contributions to the AMOC are 2.11 Sv from subduction from the Irminger Sea, 2.16 Sv from the Nordic seas, and 0.92 Sv from the Rockall basin. Of the Nordic seas component, 1.26 Sv is from the Denmark Strait, and

Unauthenticated | Downloaded 11/12/21 11:59 AM UTC

0.90 Sv is from the Faroe Bank Channel. All of the AMOC components that are related to high-latitude subduction show a similar structure to each other that extends throughout the North Atlantic to the south of the Greenland–Scotland Ridge and down to depths of about 3 km. While the peak contribution at 26°N of 0.68 Sv from the subtropical overturning cell is not insignificant, this is part of a very shallow cell. Its contribution to the peak AMOC at 881-m depth is only 0.37 Sv. Contributions from the Arctic and Mediterranean domains are very small. The negative streamlines at approximately 45°N in the Mediterranean component are associated with the circulation of the Black Sea, through which some particles entered. When interpreting these plots, it is important to bear in mind that the latitude plotted along the x axis is the mean latitude along each meridional index, which becomes increasingly curved at higher latitudes (see section 2a).

Choice of MLD threshold has differed greatly between different studies. We have chosen a threshold of $0.01\,\mathrm{kg\,m^{-3}}$ because it resembles that of the model turbulent kinetic energy scheme (Fig. 1a). There is, however, no guarantee that this correctly identifies the base of the model mixed layer. We therefore estimate the sensitivity of the results to various choices of MLD criterion: 0.001, 0.003, 0.005, 0.01, and $0.02\,\mathrm{kg\,m^{-3}}$. A higher sampling frequency at lower thresholds is chosen because the MLD is qualitatively identified as typically lying on or between the 0.003 and $0.01\,\mathrm{kg\,m^{-3}}$ thresholds, as determined through a comparison between the MLDs and the density profiles of the Irminger and Labrador Seas (not shown). We include the 0.001 and $0.02\,\mathrm{kg\,m^{-3}}$ definitions for completeness to demonstrate sensitivity outside of what is considered an acceptable range. For each of the four major contributors to the peak AMOC at 881-m depth, the range of possibilities for MLD choices from 0.003 to $0.01\,\mathrm{kg\,m^{-3}}$ are all within 20% of the contribution for an MLD choice of $0.01\,\mathrm{kg\,m^{-3}}$. We note that an inspection of the MLDs and density profiles in the Irminger and Labrador Seas suggests the model MLD more likely lies between 0.003 and $0.005\,\mathrm{kg\,m^{-3}}$. The sensitivity to MLD choice can thus likely be better constrained upon inspection of the density profiles.

It is useful to be able to relate the time taken for subduction events to impact the AMOC at a particular latitude, which is easily assessed in a Lagrangian framework according to the mean and standard deviation of propagation time between the particles' last points of subduction and 10°N (Fig. 8a). Average propagation times for water subducting from the Subpolar Gyre is typically on the order of 120 yr, decreasing to approximately 100 yr near the subpolar boundary

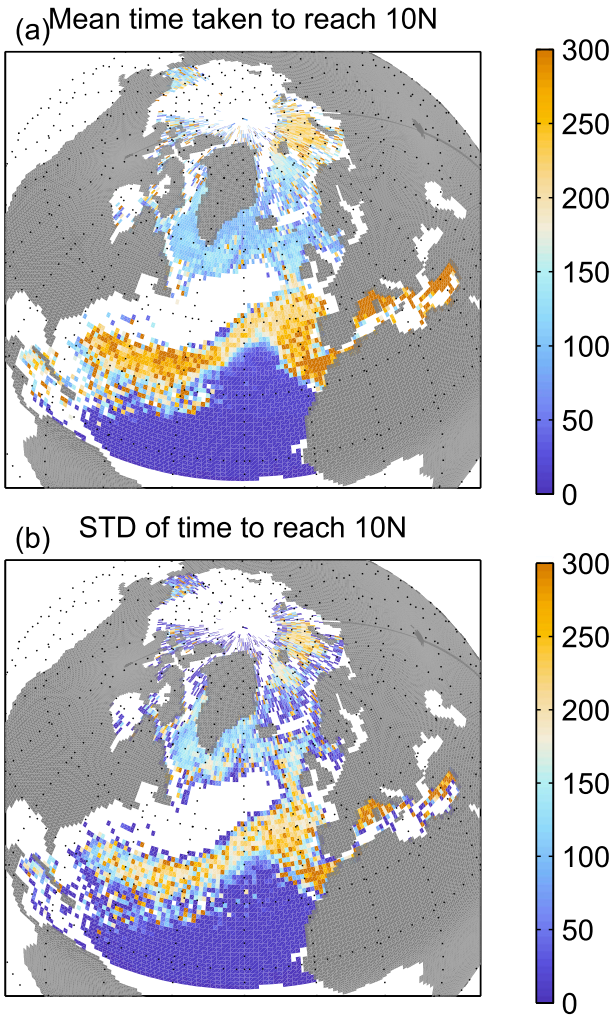

FIG. 8. (a) Time mean (yr) and (b) standard deviation of time taken (yr) for subducted water to reach 10°N. White areas indicate that the point of last subduction from the mixed layer was never from these regions.

(because of increased chance of rapid export in the deep western boundary current), and increasing to approximately 180 yr in the northern Nordic seas. Variability about this travel time is, however, of a similar magnitude to the mean (Fig. 8b). The ventilation time scales compare to existing estimates that find the age of North Atlantic Deep Water at around 10°N to be about 200 yr (e.g., England 1995; DeVries and Primeau 2011). This is higher than our subpolar ventilation time scales and perhaps indicates that the deep ocean contains more water from the Nordic seas than is represented in our model, which is likely to be unrealistically dominated by subduction from the Labrador Sea (Sarafanov et al. 2012). The longest ventilation time scales in the model are found along and slightly to the south of the Gulf Stream axis. This subduction corresponds to a deep but

Unauthenticated | Downloaded 11/12/21 11:59 AM UTC

weak overturning cell (Fig. 2i). The long time scales suggest that this water makes many transits of the gyres before then entraining into deeper flows and returning at depth. This is in line with studies that suggest water in the Subtropical Gyre must first spiral downward to intermediate depth before it can penetrate farther northward into the Subpolar Gyre (Spall 1992; Polton and Marshall 2003; Burkholder and Lozier 2011). Travel times for subducted water from the southern Subtropical Gyre are short, which probably relate to the stronger and shallow subtropical overturning cell (Fig. 2i; Table 1).

5. Discussion

The subduction components can be compared to observational estimates to help understand the model AMOC, which is approximately 4.5 Sv weaker than observations at 26°N (McCarthy et al. 2012). Observations suggest the dominant components of the AMOC come from the overflows of the Greenland–Scotland Ridge and its subsequent entrainment of ambient water, which respectively contribute 6.4 and 7 Sv to the density space AMOC at 59.5°N (Dickson and Brown 1994; Hansen et al. 2004; Sarafanov et al. 2012). Entrainment mostly occurs below the mixed layer, downstream of the Denmark Straits in the Irminger Sea. A net Irminger Sea contribution of 3.2 Sv is then the residual of this below-mixed layer entrainment and 10.2 Sv of water leaving the surface layer (Sarafanov et al. 2012). It is unknown to the authors if the relatively high rates of Irminger Sea mixed layer subduction are a direct consequence of the entrainment that occurs below it. The Labrador Sea has been estimated to contribute approximately 2 Sv to the AMOC, but estimates of this value vary greatly and could be as high as 8.5 Sv based on estimates of water mass transformation (see Table 1 in Pickart and Spall 2007).

In CNRM, only 2.16 Sv of overflow waters contribute to the AMOC streamfunction at 26°N, more than 4 Sv weaker than observed estimates. While the Irminger Sea AMOC contribution of 2.11 Sv is quite close to the net observational estimate of 3.2 Sv, it is far lower than the total estimated 10.2 Sv leaving the surface layer, which is the value that is best compared to our study. Because of the unrealistic depths and distribution of the March-mean mixed layer depths, we suggest that the Labrador Sea component of 7.51 Sv is unrealistically large. First, this is because the model distribution of maximum MLD around the edge of the Labrador Sea is where both sinking and water mass transformation has previously been found to occur (Spall and Pickart 2001; Pickart and Spall 2007), and it is also where net subduction occurs in our model (Fig. 3). Second, it is because the annual-mean mixed layer depth in the model has been found to correlate with the net subduction (see section 3), so too-deep mixed layers imply too much subduction. Therefore, in terms of AMOC contributions from mixed layer subduction, the weak model overturning is due to weak representations of both the sills overflow and the Irminger Sea subduction. This is then likely to be offset by a too-strong model representation of Labrador Sea subduction.

Our method cannot presently be used to diagnose the contribution to the AMOC from water entrained into the overflows of the Greenland–Scotland Ridge. Entrainment is typically too strong in z-coordinate ocean models, such as the one used here (e.g., Legg et al. 2006). Given its important contribution to ocean overturning, it would be useful to be able to isolate the amount and locations of entrainment in models. We propose that the method could be extended to also diagnose entrainment by identifying sudden changes in the density of particles. This could be done by applying a constraint in Ariane that terminates particle integrations when undergoing threshold changes in density in the vicinity of the overflow sills and below the mixed layer. Such a threshold could be determined by analyzing the along-track densities of particles advected near the sills (employing the so-called qualitative mode of Ariane, which outputs trajectory information). The constraint could then be used to extract the AMOC contribution from entrainment in a similar manner to that described in item 2 of section 4b above. This requires some testing that is beyond the scope of this work and is left for future iterations of the method.

There are some additional limitations of the method. First, the particle trajectories do not fully sample the spatial and temporal distribution of the model velocities, a problem that has led in this case to a slightly underestimated Lagrangian AMOC. Discrepancies between the Eulerian and Lagrangian calculations peak at about 0.6 Sv at 10°N, but they are typically less than 0.4 Sv within and to the north of the subtropics. Second, it is necessary to know the model mixed layer depth, to which the AMOC decomposition can be sensitive. Within acceptable bounds of MLD threshold choice, based on an inspection of the density profiles, we estimate a possible range of up to 20% in the component AMOC transports relative to an MLD threshold choice of 0.01 kg m^{-3} (see section 4b). Finally, our method currently extracts only the time-mean and not time-dependent AMOC. Future uses of the method could, however, be used to extract the time-dependent contribution by 1) releasing enough particles such that the sampling of both the northward and southward velocities reaches a steady state at any one

Unauthenticated | Downloaded 11/12/21 11:59 AM UTC

latitude over some duration of the simulation; 2) releasing particles into the North Atlantic from both a southern and a northern cross section (e.g., at 10° and 65°N); and 3) by instead running the particles within a global domain.

As a cautionary note for any future uses of the methodology presented here, it is important that the eddy-induced velocities of the Gent and Mcwilliams (1990) parameterization are included in Ariane if the parameterization is employed in the model. Omission of these velocities results in an erroneously strong AMOC contribution (of about 3 Sv) of the subtropical component. This appears to be because many particles are otherwise prevented from crossing into the Subpolar Gyre before returning to 10°N and are instead blocked by the Gulf Stream. Since the eddy-induced velocities of the Gent and Mcwilliams (1990) parameterization are not readily available for many of the simulations on the CMIP5 data archive, we encourage modeling centers to make these values available in future releases.

6. Conclusions

Complex ocean models are used to help understand the global circulation and influence climate policy. However, the various available model representations of the Atlantic meridional overturning circulation (AMOC), a key climate index, can be very different for reasons that can be difficult to isolate. We have developed a Lagrangian-based method to linearly decompose the AMOC according to the impacts of mixed layer subduction from different geographical regions. By tracing particle transport trajectories backward in time from 10°N to their point of last subduction from the model mixed layer, it has been possible to explicitly decompose the AMOC into component contributions. Our main purposes here have been, first, to describe the methodology and, second, to use it to decompose and explain why the CORE-II-forced CNRM ocean model AMOC of 14.03 Sv at 26°N is approximately 4.5 Sv too weak compared to observations made at the RAPID array (McCarthy et al. 2012).

We have first described the model subduction according to an Eulerian calculation. Net subduction in the model occurs primarily along the boundaries of the Subpolar Gyre and Nordic seas (Fig. 5), similar to where net sinking and water mass transformation have been found to occur (Böning et al. 1996; Spall and Pickart 2001; Pickart and Spall 2007). Net subduction is the result of strong cancellation of the spatial and temporal characteristics of obduction and subduction events (Figs. 3, 4, 5; Marshall et al. 1993; Qiu and Huang 1995; Valdivieso Da Costa et al. 2005). Integrated over the Labrador Sea, monthly peaks of net subduction that reach as high as 200 Sv in the model cancel out over the annual cycle to rates typically less than 8 Sv and a time-mean rate of 5.2 Sv.

Particles have been run backward in time from 10°N within a North Atlantic/Arctic domain that is bordered at both 10°N and at the Bering Strait. Component streamfunctions were then calculated according to a set of subdomains (the geographical boundaries of which are shown in Fig. 6) from which particles last subducted from the mixed layer. A component streamfunction was determined also for particles that recirculate back to 10°N without interacting with the mixed layer, which was dominated by Antarctic Bottom Water that describes an anticlockwise overturning circulation cell. Of a total model Lagrangian maximum AMOC of 13.92 Sv at 26°N, which occurs at 881-m depth, high-latitude subduction from the Labrador Sea, Irminger Sea, Nordic seas, and Rockall basin account, respectively, for 7.51, 2.11, 2.16, and 0.92 Sv (Fig. 7; Table 1). AMOC contributions from the Subtropical Gyre, Mediterranean Sea, and Arctic Ocean subduction are small in the model. Contributions to the AMOC from high-latitude subduction originate predominantly near the boundaries of the Subpolar Gyre and Nordic seas (Fig. 6). This is consistent with earlier estimates of where subduction occurs (Marshall et al. 1993; Valdivieso Da Costa et al. 2005), with where water mass transformation (Pickart and Spall 2007) and sinking (Böning et al. 1996; Spall and Pickart 2001) occur, and with findings that show net sinking does not occur within interior ocean convection sites (e.g., Send and Marshall 1995; Spall and Pickart 2001).

The 4.5-Sv model AMOC discrepancy to observations is accounted for by a too-weak representation of the sills overflow of the Greenland–Scotland Ridge (by approximately 4 Sv) and also by weak subduction from the mixed layers of the Irminger Sea. The weak contributions from these components are likely offset by a too-strong contribution to the AMOC from the Labrador Sea, which has previously been estimated to contribute approximately only 2 Sv to high-latitude density space overturning even during a period of intense convective activity (Pickart and Spall 2007). Reasons for the discrepancy in the AMOC between the model and observations is summarized in more detail in the discussion in section 5.

Lagrangian methods have previously been shown to be useful in decomposing and understanding the AMOC (Blanke et al. 2002; Döös et al. 2008). Eulerian methods have also been used to estimate the AMOC from surface fluxes and water mass transformation (Marshall et al. 1999; Grist et al. 2012), a framework that can also be extended to a calculation of regional impacts on AMOC.

Unauthenticated | Downloaded 11/12/21 11:59 AM UTC

The Lagrangian method presented here compliments and extends these studies, providing a powerful new way to decompose the full AMOC streamfunctions of ocean models and to directly link the strength of the overturning circulation to the geographical distribution of mixed layer subduction. Subduction strength can furthermore be related to the distribution of mixed layer depths, and its time scales of impact on the AMOC can be assessed. As such, model realism can be more directly tested against observations, and differences between models can be better understood. We propose that its application to a suite of models would give very useful insight into the differences between their respective AMOCs. Use of a high-resolution model may further give valuable insight into the 3D nature of the AMOC, particularly if particles are used to extract its temporal variability.

Acknowledgments. This work was funded by the European Commission's 7th Framework Programme, under Grant Agreement 282672, EMBRACE project. The authors gratefully acknowledge Nicolas Grima and Claude Talandier for computing support, as well as Camille Lique, Gillaume Maze, and Mary-Louise Timmermans for helpful discussions. Early discussions with Kristofer Döös were particularly appreciated. Data from the RAPID-WATCH MOC monitoring project are funded by the Natural Environment Research Council and are freely available (www.rapid.ac.uk/rapidmoc).

REFERENCES

Barnier, B., and Coauthors, 2006: Impact of partial steps and momentum advection schemes in a global ocean circulation model at eddy-permitting resolution. *Ocean Dyn.*, **56**, 543–567, doi:10.1007/s10236-006-0082-1.

Beckmann, A., and R. Döscher, 1997: A method for improved representation of dense water spreading over topography in geopotential-coordinate models. *J. Phys. Oceanogr.*, **27**, 581–591, doi:10.1175/1520-0485(1997)027<0581:AMFIRO>2.0.CO;2.

Blanke, B., and P. Delecluse, 1993: Variability of the tropical Atlantic Ocean simulated by a general circulation model with two different mixed-layer physics. *J. Phys. Oceanogr.*, **23**, 1363–1388, doi:10.1175/1520-0485(1993)023<1363:VOTTAO>2.0.CO;2.

——, and S. Raynaud, 1997: Kinematics of the Pacific Equatorial Undercurrent: An Eulerian and Lagrangian approach from GCM results. *J. Phys. Oceanogr.*, **27**, 1038–1053, doi:10.1175/1520-0485(1997)027<1038:KOTPEU>2.0.CO;2.

——, M. Arhan, G. Madec, and S. Roche, 1999: Warm water paths in the equatorial Atlantic as diagnosed with a general circulation model. *J. Phys. Oceanogr.*, **29**, 2753–2768, doi:10.1175/1520-0485(1999)029<2753:WWPITE>2.0.CO;2.

——, ——, S. Speich, and K. Pailler, 2002: Diagnosing and picturing the North Atlantic segment of the global conveyor belt by means of an ocean general circulation model. *J. Phys. Oceanogr.*, **32**, 1430–1451, doi:10.1175/1520-0485(2002)032<1430:DAPTNA>2.0.CO;2.

Böning, C. W., F. O. Bryan, W. R. Holland, and R. Doscher, 1996: Deep-water formation and meridional overturning in a high-resolution model of the North Atlantic. *J. Phys. Oceanogr.*, **26**, 1142–1164, doi:10.1175/1520-0485(1996)026<1142:DWFAMO>2.0.CO;2.

Burkholder, K. C., and M. S. Lozier, 2011: Subtropical to subpolar pathways in the North Atlantic: Deductions from Lagrangian trajectories. *J. Geophys. Res.*, **116**, C07017, doi:10.1029/2010JC006697.

Cunningham, S. A., and Coauthors, 2007: Temporal variability of the Atlantic meridional overturning circulation at 26.5°N. *Science*, **317**, 935–938, doi:10.1126/science.1141304.

Danabasoglu, G., and Coauthors, 2014: North Atlantic simulations in Coordinated Ocean-ice Reference Experiments phase II (CORE-II). Part I: Mean states. *Ocean Modell.*, **73**, 76–107, doi:10.1016/j.ocemod.2013.10.005.

de Boyer Montégut, C. D., G. Madec, A. S. Fischer, A. Lazar, and D. Iudicone, 2004: Mixed layer depth over the global ocean: An examination of profile data and a profile-based climatology. *J. Geophys. Res.*, **109**, C12003, doi:10.1029/2004JC002378.

DeVries, T., and F. Primeau, 2011: Dynamically and observationally constrained estimates of water-mass distributions and ages in the global ocean. *J. Phys. Oceanogr.*, **41**, 2381–2401, doi:10.1175/JPO-D-10-05011.1.

Dickson, R. R., and J. Brown, 1994: The production of North Atlantic Deep Water: Sources, rates, and pathways. *J. Geophys. Res.*, **99**, 12 319–12 341, doi:10.1029/94JC00530.

Döös, K., 1995: Interocean exchange of water masses. *J. Geophys. Res.*, **100**, 13 499–13 514, doi:10.1029/95JC00337.

——, J. Nycander, and A. C. Coward, 2008: Lagrangian decomposition of the Deacon Cell. *J. Geophys. Res.*, **113**, C07028, doi:10.1029/2007JC004351.

England, M. H., 1995: The age of water and ventilation timescales in a global ocean model. *J. Phys. Oceanogr.*, **25**, 2756–2777, doi:10.1175/1520-0485(1995)025<2756:TAOWAV>2.0.CO;2.

Gent, P. R., and J. C. McWilliams, 1990: Isopycnal mixing in ocean circulation models. *J. Phys. Oceanogr.*, **20**, 150–155, doi:10.1175/1520-0485(1990)020<0150:IMIOCM>2.0.CO;2.

Gregory, J. M., and Coauthors, 2005: A model intercomparison of changes in the Atlantic thermohaline circulation in response to increasing atmospheric CO_2 concentration. *Geophys. Res. Lett.*, **32**, L12703, doi:10.1029/2005GL023209.

Grist, J. P., S. A. Josey, and R. Marsh, 2012: Surface estimates of the Atlantic overturning in density space in an eddy-permitting ocean model. *J. Geophys. Res*, **117**, C06012, doi:10.1029/2011JC007752.

Hansen, B., S. Osterhus, D. Quadfasel, and W. Turrell, 2004: Already the day after tomorrow? *Science*, **305**, 953–954, doi:10.1126/science.1100085.

Hewitt, H. T., D. Copsey, I. D. Culverwell, C. M. Harris, R. S. R. Hill, A. B. Keen, A. J. McLaren, and E. C. Hunke, 2011: Design and implementation of the infrastructure of HadGEM3: The next-generation Met Office climate modelling system. *Geosci. Model Dev.*, **4**, 223–253, doi:10.5194/gmd-4-223-2011.

Holte, J., and L. Talley, 2009: A new algorithm for finding mixed layer depths with applications to Argo data and Subantarctic Mode Water formation. *J. Atmos. Oceanic Technol.*, **26**, 1920–1939, doi:10.1175/2009JTECHO543.1.

——, J. Gilson, L. Talley, and D. Roemmich, 2010: Argo mixed layers. [Available online at http://mixedlayer.ucsd.edu.]

Kanzow, T., and Coauthors, 2007: Observed flow compensation associated with the MOC at 26.5°N in the Atlantic. *Science*, **317**, 938–941, doi:10.1126/science.1141293.

Unauthenticated | Downloaded 11/12/21 11:59 AM UTC

Large, W. G., and S. G. Yeager, 2009: The global climatology of an interannually varying air–sea flux data set. *Climate Dyn.*, **33**, 341–364, doi:10.1007/s00382-008-0441-3.

Legg, S., R. W. Hallberg, and J. B. Girton, 2006: Comparison of entrainment in overflows simulated by z-coordinate, isopycnal and non-hydrostatic models. *Ocean Modell.*, **11**, 69–97, doi:10.1016/j.ocemod.2004.11.006.

Liu, L. L., and R. X. Huang, 2012: The global subduction/obduction rates: Their interannual and decadal variability. *J. Climate*, **25**, 1096–1115, doi:10.1175/2011JCLI4228.1.

Madec, G., 2008: Nemo ocean engine. IPSL Note du Pôle Modélisation 27.

Marshall, J. C., A. J. G. Nurser, and R. G. Williams, 1993: Inferring the subduction rate and period over the North Atlantic. *J. Phys. Oceanogr.*, **23**, 1315–1329, doi:10.1175/1520-0485(1993)023<1315:ITSRAP>2.0.CO;2.

——, D. Jamous, and J. Nilsson, 1999: Reconciling thermodynamic and dynamic methods of computation of water-mass transformation rates. *Deep-Sea Res. I*, **46**, 545–572, doi:10.1016/S0967-0637(98)00082-X.

McCarthy, G., and Coauthors, 2012: Observed interannual variability of the Atlantic meridional overturning circulation at 26.5°N. *Geophys. Res. Lett.*, **39**, L19609, doi:10.1029/2012GL052933.

Pickart, R. S., and M. A. Spall, 2007: Impact of Labrador Sea convection on the North Atlantic meridional overturning circulation. *J. Phys. Oceanogr.*, **37**, 2207–2227, doi:10.1175/JPO3178.1.

Polton, J. A., and D. P. Marshall, 2003: Understanding the structure of the subtropical thermocline. *J. Phys. Oceanogr.*, **33**, 1240–1249, doi:10.1175/1520-0485(2003)033<1240:UTSOTS>2.0.CO;2.

Qiu, B., and R. X. Huang, 1995: Ventilation of the North Atlantic and North Pacific: Subduction versus obduction. *J. Phys. Oceanogr.*, **25**, 2374–2390, doi:10.1175/1520-0485(1995)025<2374:VOTNAA>2.0.CO;2.

Salas-Mélia, D., 2002: A global coupled sea ice–ocean model. *Ocean Modell.*, **4**, 137–172, doi:10.1016/S1463-5003(01)00015-4.

Sarafanov, A., and Coauthors, 2012: Mean full-depth summer circulation and transports at the northern periphery of the Atlantic Ocean in the 2000s. *J. Geophys. Res.*, **117**, C01014, doi:10.1029/2011JC007572.

Send, U., and J. Marshall, 1995: Integral effects of deep convection. *J. Phys. Oceanogr.*, **25**, 855–872, doi:10.1175/1520-0485(1995)025<0855:IEODC>2.0.CO;2.

Spall, M. A., 1992: Cooling spirals and recirculation in the subtropical gyre. *J. Phys. Oceanogr.*, **22**, 564–571, doi:10.1175/1520-0485(1992)022<0564:CSARIT>2.0.CO;2.

——, and R. S. Pickart, 2001: Where does dense water sink? A subpolar gyre example. *J. Phys. Oceanogr.*, **31**, 810–826, doi:10.1175/1520-0485(2001)031<0810:WDDWSA>2.0.CO;2.

Våge, K., and Coauthors, 2009: Surprising return of deep convection to the subpolar North Atlantic Ocean in winter 2007–2008. *Nat. Geosci.*, **2**, 67–72, doi:10.1038/ngeo382.

Valdivieso Da Costa, M., and B. Blanke, 2004: Lagrangian methods for flow climatologies and trajectory error assessment. *Ocean Modell.*, **6**, 335–358, doi:10.1016/S1463-5003(03)00023-4.

——, H. Mercier, and A. M. Treguier, 2005: Effects of the mixed layer time variability on kinematic subduction rate diagnostics. *J. Phys. Oceanogr.*, **35**, 427–443, doi:10.1175/JPO2693.1.

Voldoire, A., and Coauthors, 2013: The CNRM-CM5.1 global climate model: Description and basic evaluation. *Climate Dyn.*, **40**, 2091–2121, doi:10.1007/s00382-011-1259-y.

Williams, R. G., 2001: Ocean subduction. *Encyclopedia of Ocean Sciences*, J. H. Steele, S. A. Thorpe, and K. K. Turekian, Eds., Academic Press, 1982–1993.

Wood, R. A., M. Vellinga, and R. Thorpe, 2003: Global warming and thermohaline circulation stability. *Philos. Trans. Roy. Soc. London*, **A361**, 1961–1974, doi:10.1098/rsta.2003.1245.

Zhang, L., and C. Wang, 2013: Multidecadal North Atlantic sea surface temperature and Atlantic meridional overturning circulation variability in CMIP5 historical simulations. *J. Geophys. Res. Oceans*, **118**, 5772–5791, doi:10.1002/jgrc.20390.

Unauthenticated | Downloaded 11/12/21 11:59 AM UTC